Multiwavelength campaign on Mrk 509. XIII. Testing ionized-reflection models on Mrk 509

R. Boissay, S. Paltani, G. Ponti, S. Bianchi, M. Cappi, J. S. Kaastra, P. -O. Petrucci, N. Arav, G. Branduardi-Raymont, E. Costantini, et al.

A&A 567, A44 (2014)
DOI: 10.1051/0004-6361/201423494

Astronomy & Astrophysics

Multiwavelength campaign on Mrk 509

XIII. Testing ionized-reflection models on Mrk 509

R. Boissay[1], S. Paltani[1], G. Ponti[2], S. Bianchi[3], M. Cappi[4], J. S. Kaastra[5,6], P.-O. Petrucci[7], N. Arav[8], G. Branduardi-Raymont[9], E. Costantini[5], J. Ebrero[5], G. A. Kriss[10,11], M. Mehdipour[5,9], C. Pinto[5], and K. C. Steenbrugge[12,13]

[1] Department of Astronomy, University of Geneva, ch. d'Écogia 16, 1290 Versoix, Switzerland
e-mail: rozenn.boissay@unige.ch
[2] Max-Planck-Institut für extraterrestrische Physik, Giessenbachstrasse, 85748 Garching, Germany
[3] Dipartimento di Matematica e Fisica, Università degli Studi Roma Tre, via della Vasca Navale 84, 00146 Roma, Italy
[4] INAF-IASF Bologna, via Gobetti 101, 40129 Bologna, Italy
[5] SRON Netherlands Institute for Space Research, Sorbonnelaan 2, 3584 CA Utrecht, The Netherlands
[6] Sterrenkundig Instituut, Universiteit Utrecht, PO Box 80000, 3508 TA Utrecht, The Netherlands
[7] UJF-Grenoble I / CNRS-INSU, Institut de Planétologie et d'Astrophysique de Grenoble (IPAG) UMR 5274, 38041 Grenoble, France
[8] Department of Physics, Virginia Tech, Blacksburg, VA 24061, USA
[9] Mullard Space Science Laboratory, University College London, Holmbury St. Mary, Dorking, Surrey, RH5 6NT, UK
[10] Space Telescope Science Institute, 3700 San Martin Drive, Baltimore, MD 21218, USA
[11] Department of Physics and Astronomy, The Johns Hopkins University, Baltimore, MD 21218, USA
[12] Instituto de Astronomía, Universidad Católica del Norte, Avenida Angamos 0610, Casilla 1280 Antofagasta, Chile
[13] Department of Physics, University of Oxford, Keble Road, Oxford OX1 3RH, UK

Received 23 January 2014 / Accepted 12 April 2014

ABSTRACT

Active galactic nuclei (AGN) are the most luminous persistent objects in the universe. The X-ray domain is particularly important because the X-ray flux represents a significant fraction of the bolometric emission from such objects and probes the innermost regions of accretion disks, where most of this power is generated. An excess of X-ray emission below ~2 keV, called soft-excess, is very common in Type 1 AGN spectra. The origin of this feature remains debated. Originally modeled with a blackbody, there are now several possibilities to model the soft-excess, including warm Comptonization and blurred ionized reflection. In this paper, we test ionized-reflection models on Mrk 509, a bright Seyfert 1 galaxy for which we have a unique data set, in order to determine whether it can be responsible for the strong soft-excess. We use ten simultaneous *XMM-Newton* and INTEGRAL observations performed every four days. We present here the results of the spectral analysis, the evolution of the parameters, and the variability properties of the X-ray emission. The application of blurred ionized-reflection models leads to a very strong reflection and an extreme geometry, but fails to reproduce the broad-band spectrum of Mrk 509. Two different scenarios for blurred ionized reflection are discussed: stable geometry and lamp-post configuration. In both cases we find that the model parameters do not follow the expected relations, indicating that the model is fine-tuned to fit the data without physical justification. A large, slow variation in the soft-excess without a counterpart in the hard X-rays could be explained by a change in ionization of the reflector. However, such a change does not naturally follow from the assumed geometrical configuration. Warm Comptonization remains the most probable origin of the soft-excess in this object. Nevertheless, it is possible that both ionized reflection and warm Comptonization mechanisms can explain the soft-excess in all objects, one dominating the other one, depending on the physical conditions of the disk and the corona.

Key words. galaxies: active – galaxies: nuclei – galaxies: Seyfert – galaxies: individual: Mrk 509 – X-rays: galaxies

1. Introduction

In non-obscured active galactic nuclei (AGN), most of the radiation is emitted in the optical-UV and the X-ray energy bands. In the optical-UV band, the emission is characterized by the "big blue bump", which is present from about 10 nm to 0.3 μm (Sanders et al. 1989; Bregman 1990; Zhou et al. 1997). This emission is thought to come from an optically thick accretion disk (Shakura & Sunyaev 1973).

The X-ray spectrum of Seyfert galaxies is typically characterized by a power-law continuum with reflection features, absorption, and often an excess in the soft X-rays (Halpern 1984; Turner & Pounds 1989). The power-law emission is believed to be due to the Comptonization of the UV photons coming from the disk by the energetic electrons in a corona surrounding the disk (Blandford et al. 1990; Zdziarski et al. 1995, 1996; Krolik 1999). As a high-energy cut-off is detected in a range from about 80 to 300 keV in about 50% of Seyfert galaxies, a thermal distribution is preferred to a non-thermal one (Gondek et al. 1996; Matt 2001; Perola et al. 2002).

The strongest signatures of the reflection component are a "reflection hump" around 30 keV and an iron FeKα fluorescence line in between 6 and 7 keV depending on the iron ionization state. Reflection is associated with the reprocessing of the primary continuum by material either close to the central black hole, in the accretion disk (George & Fabian 1991; Matt et al. 1991), or more distant, for example in a torus (Antonucci 1993; Jaffe et al. 2004; Meisenheimer et al. 2007; Raban et al. 2009).

It can also be produced either in the narrow- or broad-line regions (Ponti et al. 2013).

Absorption from material either in the vicinity of AGN or in the host galaxy is generally observed in the X-ray spectra of Seyfert 1 and 2 galaxies. If the absorbing material is often photoionized, it is referred to as "warm absorber" (George et al. 1998).

More than 50% of Seyfert 1 galaxies show the presence of a soft X-ray excess called soft-excess (Halpern 1984; Turner & Pounds 1989), a soft X-ray emission below ~2 keV in excess of the extrapolation of the hard X-ray continuum. Piconcelli et al. (2005) and Bianchi et al. (2009) even found that the fraction of AGN with soft-excess reaches about 100%. The discovery of this component was made thanks to the HEAO-I (Singh et al. 1985) and EXOSAT (Arnaud et al. 1985) missions in the 80's, but its nature is still uncertain. It was first thought to arise from the hottest part of the accretion disk (e.g. Arnaud et al. 1985; Pounds et al. 1986), but this hypothesis was invalidated by the facts that the temperature of the soft-excess (0.1–0.2 keV) is much too high to be explained by the standard accretion disk model around a supermassive black hole and that it does not vary, as expected, with the mass of the black hole (Gierliński & Done 2004).

Another possible explanation is "warm" Comptonization: up-scattering of seed disk photons in a Comptonizing medium that has a temperature of about 1 keV (e.g., in NGC 5548 – Magdziarz et al. 1998; RE J1034+396 – Middleton et al. 2009; RX J0136.9–3510 – Jin et al. 2009; Ark 120 – Matt et al. 2014; and 1H 0419–577 – Di Gesu et al. 2014). This Comptonization model is supported by strong similarities having been found in the optical-UV and soft X-ray variability, suggesting a correlation between these emissions, in agreement with inverse-Compton processes (Edelson et al. 1996; Mehdipour et al. 2011). Walter & Fink (1993) used a sample of 58 Seyfert 1s observed by ROSAT and IUE and found a spectral shape correlation (i.e., an amplitude correlation) indicating that the soft-excess could be the high-energy tail of the "big blue bump" component observed in UV, since objects with a large UV bump also show a strong soft-excess. Edelson et al. (1996) found a correlation between variabilities in X-rays, UV, and optical bands in NGC 4151. Marshall et al. (1997) studied NGC 5548 in the extreme UV band using EUVE and noticed that the EUV and UV/optical variations of the light curves are simultaneous. They also found that the shape of the EUVE spectrum is consistent with the one in UV and soft X-rays.

The warm Comptonization model still, however, does not explain why the shape of the soft-excess does not appear to vary with the black-hole mass (Gierliński & Done 2004). An alternative explanation is that the soft-excess is linked to atomic processes. It could be the signature of strong, relativistically smeared, partially ionized absorption in a wind from the inner disk. Gierliński & Done (2004) applied this model to PG 1211+143. If a totally covering absorber is assumed, the problem of this model is that it needs very extreme values of the model parameters to account for the observed smooth soft-excesses, in particular a very high smearing velocity, which is not attainable in models of radiatively driven accretion disk winds with typical physical parameters (Schurch & Done 2007; Schurch et al. 2009). This problem no longer applies in the case of a partial-covering scenario. In Mrk 766, for example, the principal components analysis and spectral variability of a long *XMM-Newton* observation can be explained by ionized absorption partially covering the continuum source (Miller et al. 2007). Turner & Miller (2009) present a review of X-ray absorption and reflection in AGN, showing that partial-covering absorption can explain spectral curvature and variability at low energy.

Another interpretation is that the soft-excess is the result of ionized reflection in a relativistic disk, which blurs all emission lines. An ionized-reflection model, calculated for an optically thick atmosphere of constant density illuminated by radiation of a power law (called *reflionx* in XSPEC; Ross & Fabian 2005), has been successfully applied by Crummy et al. (2006) to 22 Type-1 PG quasars and 12 Seyfert 1 galaxies and by Zoghbi et al. (2008) on Mrk 478 and EXO 1346.2+2645. This model has also been applied in MCG-6-30-15 by Vaughan & Fabian (2004) and NGC 4051 by Ponti et al. (2006), explaining the spectral shape, as well as the variability. The spectral and timing analysis of 1H 0707-495 (Fabian et al. 2009) provides strong evidence of emission from matter close to a rapidly spinning black hole. This object shows the presence of a broad iron K line whose width and shape is a signature of the strong gravity and spin of the black hole. Thanks to the high iron abundance, the iron L line is also detectable, and a lag of about 30 s with the direct X-ray continuum could be measured. This lag is evidence of reverberation processes. X-ray reverberation time delays have also been detected in MCG–5–23–16 and NGC 7314 by Zoghbi et al. (2013) using the iron Kα emission lines. Kara et al. (2013) also found iron K lags in Ark 564 and Mrk 335. Soft X-ray reverberation lags have been found in ESO 113-G010 by Cackett et al. (2013) and PG 1211+143 by De Marco et al. (2011). Overall, soft lags have been found in more than 15 sources (De Marco et al. 2013). Blurred ionized reflection has also been tested, as well as double Comptonization and ionized absorption by a high-velocity material, in Mrk 509 and Mrk 841, using average broad-band Suzaku data (Cerruti et al. 2011). This model seems to correctly describe Mrk 509 soft-excess, but underestimates the broad iron emission line.

In this paper, we focus on testing blurred ionized-reflection models in an object for which we have a unique data set: Mrk 509. We want to check whether ionized reflection could be a viable alternative explanation to the warm Comptonization to explain the soft-excess. To test these ionized-reflection models, we used the Mrk 509 *XMM-Newton* and INTEGRAL campaign and its ten simultaneous observations (Kaastra et al. 2011). We first study the variability at different time scales and then we test blurred ionized-reflection models on the ten observations in order to investigate the evolution of the *reflionx* parameters.

The paper is organized as follows. In Sect. 2, we first introduce the properties of Mrk 509 and the *XMM-Newton*/INTEGRAL campaign of observation that we use. In Sect. 3, we show the results of the study of variability on different time scales. Section 4 presents the ionized-reflection models that we use to fit our data, as well as the results for the average spectrum and for each observation. In Sect. 5, we show the evolution of *reflionx* parameters, taking two cases into account: the case of a stable geometry with a constant reflection factor and the case of a varying reflection factor. All these results are discussed in Sect. 6, and we state the conclusions in Sect. 7.

2. Mrk 509 – *XMM-Newton*/INTEGRAL campaign

Mrk 509 is a bright Seyfert 1 galaxy. It has a redshift of 0.034 (Huchra et al. 1993). Its black-hole mass $M_{\rm BH} = 1.43 \times 10^8\ M_\odot$ has been determined using the reverberation mapping method (Peterson et al. 2004). This object presents a strong soft-excess, as shown in Fig. 1.

Mrk 509 has been one of the first AGN to be studied, thanks to its brightness, with a flux between 2 keV and 10 keV of

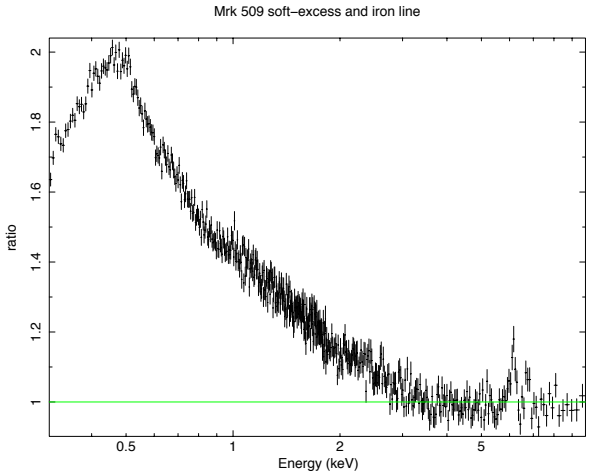

Fig. 1. Ratio to the power-law fit between 3 and 10 keV showing the presence of a strong soft-excess below 2 keV and a resolved iron line at 6.4 keV in the average spectrum of Mrk 509 (431 ks of *XMM-Newton* exposure).

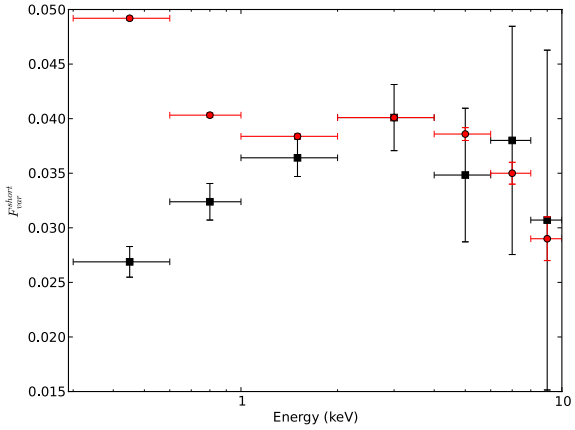

Fig. 2. Fractional variability as a function of energy. The black squares represent the variability spectrum on short time scale, $F_{\rm var}^{\rm short}$ (1 ks $\lesssim T \lesssim$ 60 ks); the red circles are the corresponding variability values predicted from the long time scale variability spectrum, $F_{\rm var}^{\rm long}$ (60 ks $\lesssim T \lesssim$ 1 month).

$F_{2-10\,\rm keV} = 2{-}5 \times 10^{-11}$ erg cm^{-2} s^{-1} (Kaastra et al. 2011). Its bolometric luminosity is $L_{\rm Bol} = 1.07 \times 10^{45}$ erg s^{-1} (Woo & Urry 2002) and it has an X-ray luminosity of $L_{\rm X} = 3 \times 10^{44}$ erg s^{-1} for energies between 2 and 10 keV (Pounds et al. 2001). The accretion rate $\dot{M}$ has a range between 20% and 30% of the Eddington rate (Petrucci et al. 2013) during the *XMM-Newton* campaign presented in Kaastra et al. (2011). The first detection in the 2 keV to 10 keV band was made with Ariel V (Cooke et al. 1978). The soft-excess was first identified in this object thanks to HEAO1-A2 (Singh et al. 1985); the iron line was detected for the first time in 1987 with EXOSAT (Morini et al. 1987), and the reflection component was initially revealed by Ginga (Pounds et al. 1994). EPIC data from *XMM-Newton* observations (in 2000, 2001, 2005, and 2006) show evidence of a complex Fe K emission line, with a narrow and a neutral component possibly produced far from the source, plus a broad and variable component possibly originating in the accretion disk (Pounds et al. 2001; Page et al. 2003; Ponti et al. 2009, 2013). Using *XMM-Newton* observations of Mrk 509, Cappi et al. (2009) detected the presence of lines, at ~8–8.5 keV and ~9.7 keV, consistent with being produced by Fe Kα and Kβ shell absorptions associated with mildly relativistic and variable outflow. These variable features were not observed during the 2009 campaign (Ponti et al. 2013).

Mrk 509 has been observed during a multiwavelength campaign presented in Kaastra et al. (2011), using five satellites, *XMM-Newton*, INTEGRAL, *Chandra*, HST, and *Swift*, and two ground-based facilities: WHT (optical imaging with Sloan g, r, i and Z filters) and PAIRITEL (infrared imaging in J, H, and K bands). Using the *XMM-Newton*, *Swift*, HST, and FUSE observations, Mehdipour et al. (2011) shows that the soft X-ray excess varies in association with the thermal optical-UV emission from the accretion disk, suggesting that the soft-excess is due to Comptonization process. Petrucci et al. (2013) used the *XMM-Newton* and INTEGRAL observations of Mrk 509 to model the broad-band emission of this object using physical models and could explain the entire optical-to-hard X-ray emission by assuming the existence of an accretion disk, a hot, optically-thin corona, responsible of the primary continuum emission, plus a warm ($kT \sim 1$ keV), optically-thick ($\tau \sim 10{-}20$) plasma, creating the optical-UV to soft X-ray emission, plus reflection on distant, neutral material. As in Petrucci et al. (2013), we use the ten simultaneous *XMM-Newton* (600 ks) and INTEGRAL (1.2 Ms) observations, performed every four days in October/November 2009, which enable us to study variability and spectra of Mrk 509 from 0.3 keV up to 200 keV (see Table 1 from Kaastra et al. 2011).

3. Variability spectra

Taking advantage of the intensive monitoring with *XMM-Newton*, we first estimate the variability spectra. We calculate the rms fractional variability amplitude, $F_{\rm var}$, following Vaughan et al. (2003):

$$F_{\rm var} = \sqrt{\frac{S^2 - \overline{\sigma_{\rm err}^2}}{\bar{x}^2}} \tag{1}$$

with $\bar{x}$ the arithmetic mean of the fluxes, $\overline{\sigma_{\rm err}^2} = \frac{1}{N}\sum_{i=1}^{N}\sigma_{{\rm err},i}^2$ and $S^2 = \frac{1}{N-1}\sum_{i=1}^{N}(x_i - \bar{x})^2$.

We calculate the rms fractional variability on two different time scales to determine the variability amplitude in Mrk 509 light curves. The variability spectrum on time scales 1–60 ks is shown in Fig. 2. We first extract light curves with bin size of 1 ks from *XMM-Newton* data and calculate rms fractional variability in different energy bands (0.3–0.6 keV, 0.6–1 keV, 1–2 keV, 2–4 keV, 4–6 keV, 6–8 keV, and 8–10 keV) for each observation. We then calculate the quadratic mean value over the ten observations to get $F_{\rm var}^{\rm short}$. The error bars represent uncertainties at 1σ level.

To obtain the variability on longer time scales, we use the average count rates in the seven energy bins of each observation. We then calculate $F_{\rm var}^{\rm long}$ for all ten observations. Since observations are averaged over 60 ks and spread over one month, $F_{\rm var}^{\rm long}$ is sensitive to time scales between ~60 ks and ~1 month. If we assume that the observed flux is the sum of a variable component – the power-law component – and a less variable component, the reflection, we can scale the $F_{\rm var}^{\rm long}$ values to the $F_{\rm var}^{\rm short}$ value at 3 keV. These new values are represented in Fig. 2.

We can see in Fig. 2 that, on short time scales, $F_{\rm var}^{\rm short}$ is maximum between 2 keV and 4 keV. The fractional variability decreases in the soft part and is consistent with a decrease in the hard part. Assuming that reflection varies less than the power law (Miniutti & Fabian 2004) and that the soft-excess is due to

ionized reflection, the variability spectrum is exactly what would be expected, since the variability on short time scales is higher where the power law dominates.

The shape of the variability spectrum on long time scales matches the one on short time scales, but there is clear excess at low energy. It shows that the soft-excess is more variable than the power law on long time scales. No variability excess is observed at high energy on long time scales, unlike what would be expected if soft-excess and reflection are a single component with no variations in spectral shape (e.g., changes of the ionization parameter should mostly affect the flux in the soft X-ray energy band). The excess of variability in the soft-excess is not compatible with the hypothesis of reflection of hard X-rays, unless the reflection parameters change.

4. Fits with ionized-reflection models

4.1. Model

Relativistically blurred ionized reflection has been proposed in several AGN as the origin of the soft-excess. Indeed, iron lines with relativistic profiles have been found in several sources (e.g., in MCG–6–30–15; Tanaka et al. 1995), as well as iron lines with very extended red wings (e.g., Nandra et al. 1997). Disk reflection models use these features to reproduce the emission from a photoionized accretion disk around a supermassive black hole (Ross & Fabian 1993, 2005; Ballantyne et al. 2001b). These models have been tested successfully in many objects (e.g., on five NLS1 by Ballantyne et al. 2001a; on 1H 0707–495 by Fabian et al. 2002; on MCG–6–30–15 by Ballantyne et al. 2003; and on 34 sources by Crummy et al. 2006, using the *reflionx* model from Ross & Fabian 2005). Nevertheless, alternative models can also explain the soft-excess in some of these AGN (e.g., warm Comptonization in Ark 564 – Dewangan et al. 2007, and PKS 0558–504 – Papadakis et al. 2010; partial covering in 1H 0707–495 – Tanaka et al. 2004; and MCG-6-30-15 – Miller et al. 2008).

In Mrk 509, the complex iron line at ~6.4 keV is decomposed into a narrow line, which is constant on a several-year time scale, probably originating in remote neutral material (see De Rosa et al. 2004; Ponti et al. 2009, 2013) and a resolved component, varying with the continuum on a time scale of a few days (Ponti et al. 2013), which is most probably produced in the broad line region or outer disk. The ionized FeK line (6.7–6.97 keV) might be produced in the inner accretion disk. To model the strong soft-excess, we use a *reflionx* component as in Crummy et al. (2006). We convolve the given reflected emission with the Laor model shape (*kdblur*; Laor 1991) to simulate the blurring from a relativistic accretion disk around a black hole.

In addition to this blurred ionized reflection, we model the power-law continuum produced by Comptonization, including a cut-off at high energy, using the *cutoffpl* component, as *reflionx* assumes a power law. To model the narrow component of the iron line, we introduce neutral Compton reflection from distant material (such as the molecular torus postulated in unification models), using the *pexmon* model (Nandra et al. 2007). This model is similar to the *pexrav* model (Magdziarz & Zdziarski 1995), but with self-consistent Fe and Ni lines and Compton shoulder (George & Fabian 1991). Complex absorption is visible in the RGS spectra of Mrk 509 (Detmers et al. 2011). We therefore add a "warm absorber" component to our model, because the gas is photoionized in our object. The final complete model is

*warm absorber (cutoffpl + pexmon + kdblur*reflionx).*

The model we apply is a complicated one, with many degrees of freedom, so we put constraints on this model and fixed some parameters. The warm absorber used for this fitting of Mrk 509 has fixed parameters that have been derived from the 600 ks RGS spectrum (Detmers et al. 2011). It includes all sources of absorption, including the Galaxy. This model of Detmers et al. (2011) has already been used in Pinto et al. (2012) and Petrucci et al. (2013). Assuming that neutral reflection originates in distant material, we chose to fix all parameters of the *pexmon* model to the values found in the average spectrum (photon index, reflection factor, abundances and inclination) for the fitting of the ten individual observations. The cut-off energy is fixed to 500 keV, because the *reflionx* model assumes a pure power-law. This will not affect the modeling using blurred reflection since the cut-off energy is >200 keV (Petrucci et al. 2013) during this campaign. In this way, many parameters of *reflionx* are fixed, the free remaining parameters for the individual fits are then the normalization and ionization parameter of the *reflionx* component, the normalization and photon index of the cut-off power-law, the index, and inner radius of the *kdblur* model.

4.2. Average spectrum

To test blurred ionized-reflection models to explain the soft-excess in Mrk 509, we fit the average spectrum of the ten *XMM-Newton* and INTEGRAL observations with the complete model. The top panel of Fig. 3 shows the average spectrum with the resulting fit and the different components of the model, and Table 1 contains the corresponding parameter values.

Abundances of iron and other elements are fixed to the solar value (Morrison & McCammon 1983). The fit on the average spectrum gives an inclination angle of the disk of 56 degrees. The illumination index of the *kdblur* model, characterizing the incident flux distribution, has a very high value of 10. The inner radius also reaches the extreme value of 1.235 GM/c^2. These two parameters imply that reflection takes place very close to the central black hole and that this one is rotating with maximal spin. Both these parameters are in fact reaching the model limits of *kdblur* in XSPEC.

Cerruti et al. (2011) tested blurred ionized-reflection models on Mrk 509, using a single-epoch Suzaku spectrum. They found that, when using *reflext* (an older version of *reflionx*) and *reflionx* models, blurred ionized reflection correctly describes the soft-excess, but underestimates the broad iron emission line, as in our model. The resulting parameters of this paper are similar to ours, except for the value of the disk emissivity index, which equal to 3 in this case. They chose to freeze all *kdblur* parameters to constrain the model and to prevent parameters from reaching the model limits. After freeing the emissivity index parameter, the best-fit value stays consistent with 3. We tried to first freeze the emissivity index to 3 and then to let it vary, but even in this case the parameter still reaches the model limit of 10.

We obtain a reduced χ^2 around 2.58 for 1340 degrees of freedom, significantly worse than what is obtained with a warm Comptonization model. Indeed, by fitting the 0.3–100 keV spectrum with the model used by Petrucci et al. (2013), but replacing the *compPS* component by a *cutoffpl* model (see bottom panel of Fig. 3), we obtain a reduced χ^2 around 2.27 for 1338 degrees of freedom (F-test probability equal to 2×10^{-38}). We note that the INTEGRAL spectrum is not well fit by an ionized-reflection model, unlike when a warm Comptonization model is used instead (see bottom panel of Fig. 3). Furthermore, the emission is dominated by a very strong reflection, which nevertheless

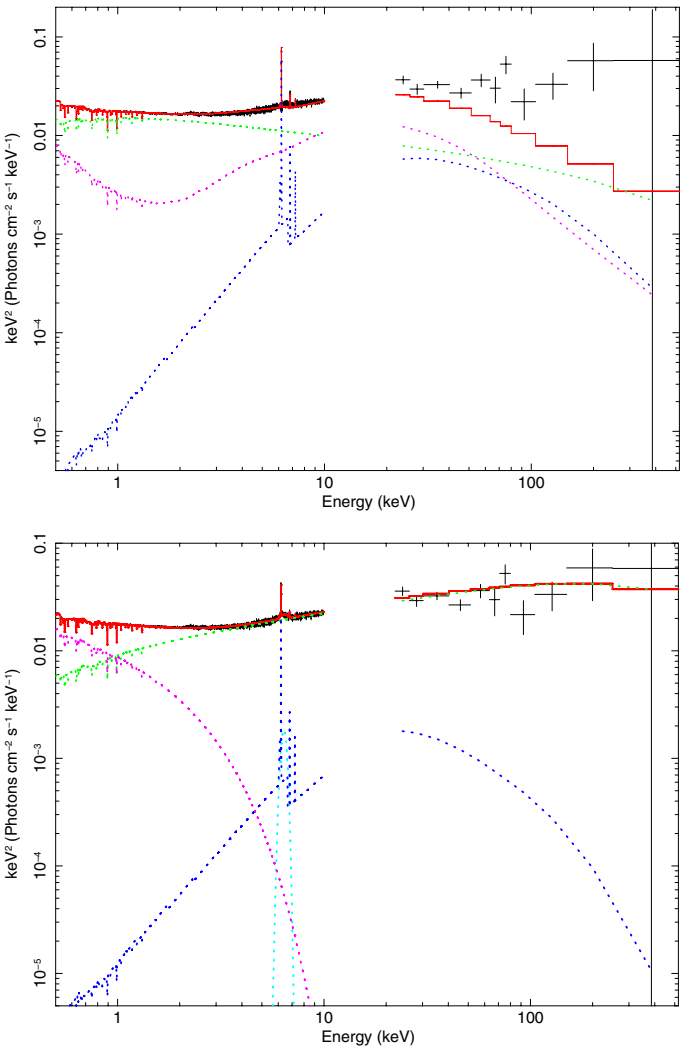

Fig. 3. Average *XMM-Newton* and INTEGRAL spectrum of Mrk 509 in XSPEC; *Top panel*: data are in black, ionized-blurred reflection fitting result is in red and components of the fitting model are in dash lines (cutoffpl: green, pexmon: blue, kdblur*reflionx: pink); *Bottom panel*: data are in black, warm Comptonization fitting result is in red and components of the fitting model are in dash lines (cutoffpl: green, pexmon: dark blue, zgauss: light blue, nthcomp: pink).

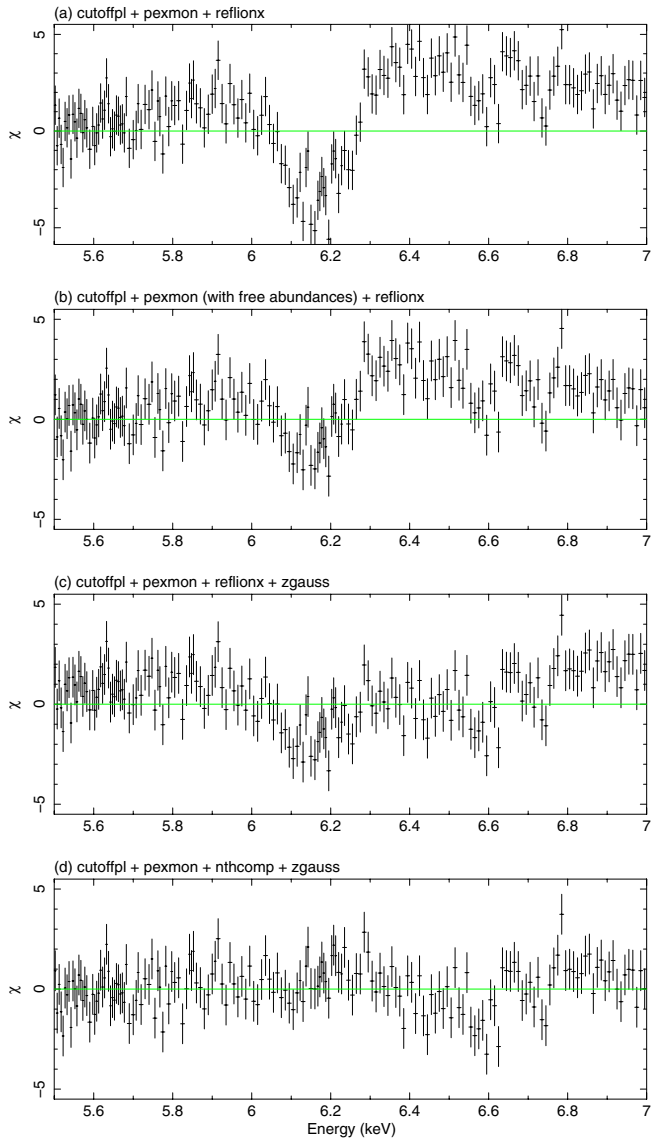

Fig. 4. Delta χ^2 obtained by fitting data with the following models of reflection and Comptonization: (a) *cutoffpl + pexmon + reflionx*; (b) *cutoffpl + pexmon* (with free abundances) + *reflionx*; (c) *cutoffpl + pexmon + reflionx + zgauss*; (d) *cutoffpl + pexmon + nthcomp + zgauss*.

Table 1. Results of the fitting of the average spectrum.

Model	Parameter	Value
Cutoffpl – Reflionx	PhoIndex	2.24 ± 0.006
Cutoffpl – Pexmon	HighECut	500 keV *
Cutoffpl – Pexmon	Normalization	$1.74 \pm 0.03 \times 10^{-2}$
Pexmon	PhoIndex	2.11 ± 0.01
Pexmon	Rel Refl	0.79 ± 0.03
Pexmon	Abund	1.00 *
Pexmon – Reflionx	Fe abund	1.00 *
Pexmon – Kdblur	Incl	56.31 ± 0.45 deg
Kdblur	Index	10.00 ± 0.45
Kdblur	Rin(G)	1.235 ± 0.02 r_g
Kdblur	Rout(G)	100.00 r_g *
Reflionx	Xi	27.27 ± 1.73 erg cm s^{-1}
Reflionx	Normalization	$4.64 \pm 0.75 \times 10^{-5}$

Notes. Parameters with the symbol * are fixed. Normalizations are given in photons keV^{-1} cm^{-2} s^{-1} at 1 keV. Abundances are relative to solar value (Morrison & McCammon 1983).

underestimates the power-law-like INTEGRAL spectrum. This bad fit is discussed further in Sect. 6.1.

Figure 4 shows fit residuals between 5.5 and 7 keV for different models. Panel a shows the ionized-reflection model used in this paper. We note that the iron line and the continuum around the line are not well fit. We obtained a slightly better fit, as shown in panel b, by leaving the abundances of iron and other elements in the *pexmon* component free, but in this case, the iron abundance is very low (28% of the solar value), and the *pexmon* model dominates the spectrum at high energy. In addition, the fit remains unsatisfactory. Panel c shows the result for the ionized-reflection model to which a Gaussian function has been added in order to represent the broad iron emission line possibly originating in the outer part of the accretion disk, similar to Petrucci et al. (2013). We fixed the photon index of the *pexmon* to the one of the power law to prevent the fit from converging on a very hard $\Gamma = 1.4$ to better fit the high-energy spectrum. We can see that the fit is better around the iron emission line, but to the detriment of the high energy. However, the fit is still unsatisfactory.

Table 2. Results of the fitting of the average spectrum and each of the ten individual observations.

Spectrum	Photon index	*Cutoffpl* normalization (10^{-2} ph keV^{-1} cm^{-2} s^{-1})	Index	Rin (r_g)	ξ (erg cm s^{-1})	*Reflionx* normalization (10^{-5} ph keV^{-1} cm^{-2} s^{-1})	χ^2/ d.o.f.
Average	2.24 ± 0.01	1.74 ± 0.03	10.00 ± 0.45	1.235 ± 0.02	27.27 ± 1.73	4.64 ± 0.75	3455/1340
1	2.19 ± 0.02	1.51 ± 0.03	10.00 ± 1.47	1.235 ± 0.09	26.24 ± 2.97	3.79 ± 0.57	602/473
2	2.22 ± 0.01	1.64 ± 0.02	10.00 ± 1.20	1.235 ± 0.08	22.12 ± 1.09	5.29 ± 0.42	742/504
3	2.26 ± 0.01	1.88 ± 0.03	10.00 ± 1.24	1.235 ± 0.08	27.09 ± 3.09	5.08 ± 0.45	714/516
4	2.32 ± 0.01	1.46 ± 0.02	10.00 ± 1.11	1.235 ± 0.07	25.17 ± 1.93	5.90 ± 0.41	723/470
5	2.32 ± 0.01	1.78 ± 0.03	10.00 ± 0.59	1.235 ± 0.07	30.48 ± 3.76	5.47 ± 0.42	739/508
6	2.20 ± 0.02	1.84 ± 0.04	10.00 ± 1.19	1.235 ± 0.08	26.87 ± 3.01	5.06 ± 0.44	730/535
7	2.27 ± 0.01	1.89 ± 0.02	10.00 ± 0.53	1.235 ± 0.08	21.75 ± 0.98	6.85 ± 0.43	746/516
8	2.17 ± 0.01	1.91 ± 0.03	10.00 ± 1.45	1.235 ± 0.09	35.78 ± 4.30	3.00 ± 0.25	769/535
9	2.25 ± 0.01	1.69 ± 0.02	10.00 ± 1.20	1.235 ± 0.08	24.53 ± 1.48	5.20 ± 0.39	729/515
10	2.17 ± 0.01	1.77 ± 0.03	10.00 ± 1.31	1.235 ± 0.08	31.05 ± 4.50	3.70 ± 0.46	662/532

Notes. All *pexmon* parameters have been fixed to the values of Table 1.

A possible explanation is that the *reflionx* model adds a hugely flattened iron line (barely visible in Fig. 3) that curves the continuum in a way that is incompatible with the data. Panel d shows a similar zoom on the iron line using the model discussed in Petrucci et al. (2013), which includes a broad iron line to mimic reflection on the accretion disk, but with a single cut-off power law to represent the continuum, instead of a physical model of Comptonization, for better comparison with the *reflionx* cases. It can be seen that the Comptonization model gives a significantly better fit to the iron line, near continuum and also at high energy.

4.3. Reflionx fits to the individual observations

As discussed in Sect. 4.1, we chose to fix all parameters of the *pexmon* model to the values found in the average spectrum and presented in Table 1. Results of the individual fits are presented in Table 2. By fitting the observations individually, we obtain a mean reduced χ^2 around 1.40 for ~510 degrees of freedom. The result with a blurred-reflection model is worse than the one obtained with the warm Comptonization model, which has a mean reduced χ^2 around 1.31 for ~504 degrees of freedom. To be able to compare these two models, we replace the *compPS* component used by Petrucci et al. (2013) to model the continuum by a cut-off power law *cutoffpl* (parameters of the *Nthcomp* model are similar to those listed in Table 2 from Petrucci et al. 2013).

Even though the χ^2 is significantly better with the Comptonization model, we do not simply discard the blurred-reflection model. Indeed, the model may be oversimplified in a number of ways. We instead focus on the values we find for the fit parameters and on the relationships they have with each other. We use a simple cut-off power-law model to represent the continuum produced by Comptonization. Unlike *compPS* (Poutanen & Svensson 1996), used by Petrucci et al. (2013), which is a physical model of Comptonization, a cut-off power law is a poor approximation of thermal Comptonization. Nevertheless, we choose *cutoffpl* instead of the *compPS* model because *reflionx* assumes a power law and because we are not interested in Comptonization details, since the aim of this project is to test ionized-reflection models.

The emissivity index and the inner radius of the *kdblur* model do not change over the ten observations and keep the extreme values found in the average spectrum.

The ionization parameter $\xi = \frac{L}{nr^2}$ erg cm s^{-1}, with L the luminosity of the ionizing source, r the distance of this source to the reflecting medium, and n the density of the illuminated gas, is in weighted-average equal to 24 erg cm s^{-1} (see top panel of Fig. 5). Such a low value seems at odds with the result that the reflecting medium is located very close to the irradiating source. This is further discussed in Sect. 6.1.

Middle panel of Fig. 5 shows the power-law flux measured between 2 keV and 10 keV for each observation. The error bars, representing uncertainties at 1σ level, are very small. The bottom panel presents the ratio of the reflected flux (0.1–50 keV) over the power-law flux as a function of the continuum power-law flux, showing a significant anticorrelation (Spearman correlation coefficient: $r = -0.56$; null-hypothesis probability: $p = 0.09$). As for the anticorrelation found, in Fig. 7 from Fabian et al. (2005), between the reflection factor (i.e., the reflection-dominated component flux relative to the power-law flux) and the continuum flux, our result can be explained by the light-bending model proposed by Miniutti & Fabian (2004). Indeed, in this configuration, the reflection is expected to vary less than the power law, which is consistent with the behavior of the short time scale variability (Fig. 2), and when the power-law flux drops the spectrum becomes more and more reflection-dominated.

5. Evolution of *reflionx* parameters

5.1. Determination of the R* parameter for reflionx

The normalization of the reflected emission component is not related to that of the incident flux, in contrast to most reflection models (*pexrav, pexriv, pexmon*). This keeps it from being straightforward for directly determining the amplitude of the reflection compared to that of the illuminating flux. The *pexriv* model describes the reflection of exponentially cut-off power-law spectrum on ionized material (Magdziarz & Zdziarski 1995). To study the evolution of *reflionx* parameters, we first want to determine the equivalent of the reflection factor R of *pexriv* for *reflionx*. We thus define the pseudo-reflection factor R^* for *reflionx*. It is a measure of the flux reflected by a reflector with a given ionization, which produces the same observed hard X-ray flux as predicted with a *pexriv* model with reflection parameter $R = R^*$ ($R = 1$ for a reflector with a solid angle of 2π).

To determine R^*, we simulate several *cutoffpl* + *reflionx* spectra with values of the parameters found in the ten fits with the complete model and fit them with a *pexriv* model. This *pexriv* model contains an explicit reflection factor and an ionization parameter, and its normalization is the power-law normalization.

Pexriv does not incorporate the many atomic transitions found at low energy in *reflionx*. However, the high-energy

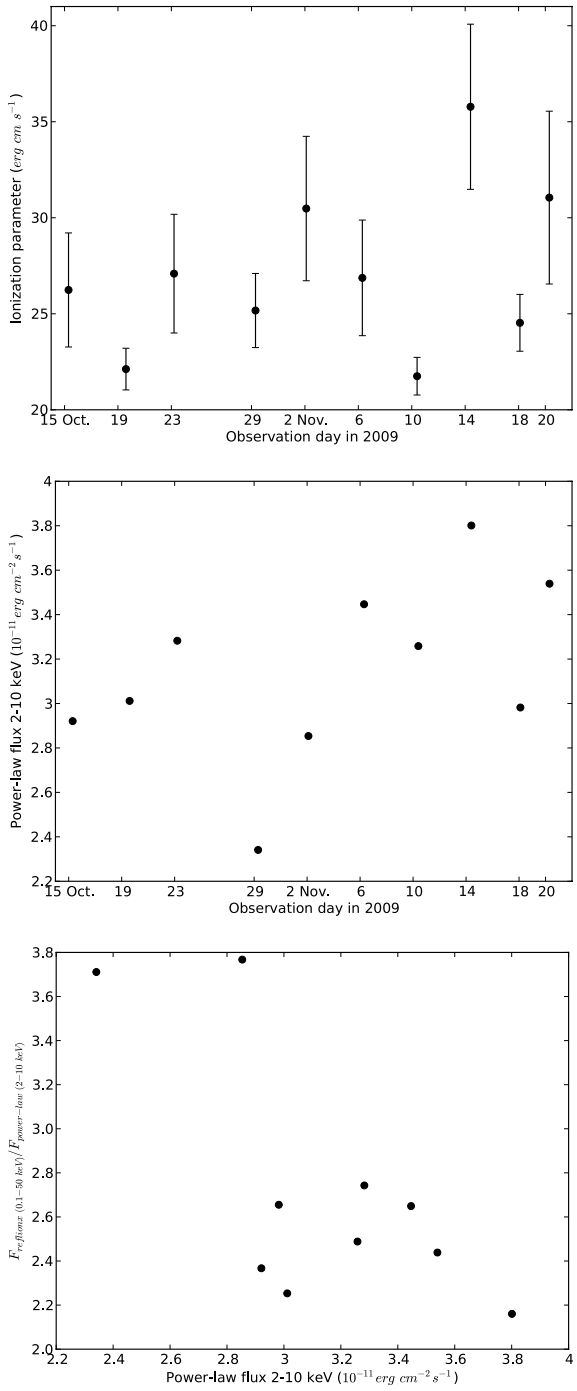

Fig. 5. Evolution of the fit parameters. *Top and middle panels*: ionization parameter and power-law flux determined for each of the ten observations. *Bottom panel*: ratio of the reflected flux (0.1–50 keV) over the power-law flux (2–10 keV), as a function of the power-law flux (2–10 keV).

properties (above 20 keV) should be similar to those of *reflionx*. The equivalent reflection factor R^* for *reflionx* is then obtained by fitting *pexriv* to the simulated power law plus *reflionx* models between 20 and 50 keV, the reflection parameter of *pexriv* then giving the R^* parameter of *reflionx*.

5.2. The case of constant R*

We first make the reasonable hypothesis of a stable geometry for Mrk 509, implying a constant reflection factor. We applied

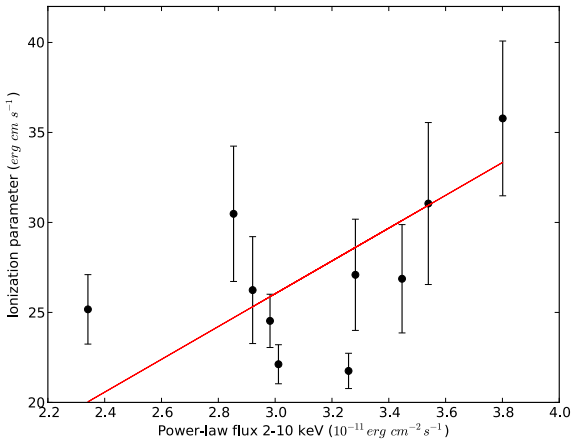

Fig. 6. Ionization parameter as a function of the power-law flux. Red line: evolution expected with fixed R^*; Black points: parameters obtained in the ten individual fits.

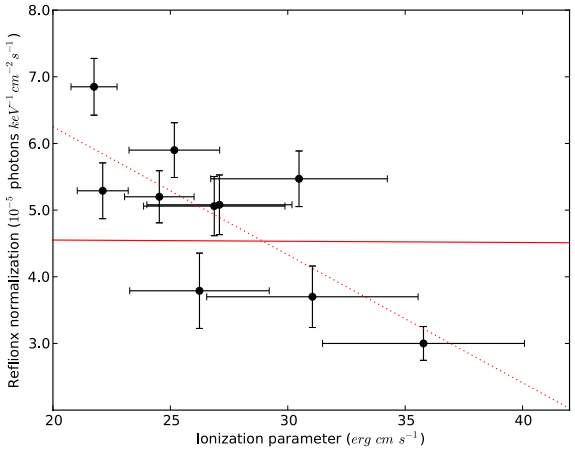

Fig. 7. Reflionx normalization as a function of the ionization parameter. Solid red line: evolution expected with a *reflionx* model. Dotted red line: expected evolution of the normalization if the power-law flux is fixed. Black points: parameters obtained by fitting data with the complete model.

the method described in Sect. 5.1 to the average spectrum of the ten observations to determine the reflection factor R^* and get $\langle R^* \rangle = 5.08 \pm 0.82$.

Figure 6 shows the ionization parameter, obtained by fitting each observation with the complete model, as a function of the 2 to 10 keV power-law flux. The figure also indicates the relation $\xi = \frac{L}{nr^2}$ that we expect with our assumption of a constant R^*, calculated by fixing R^* to the value of the average spectrum $\langle R^* \rangle = 5.08$.

The ionization parameter shows a scatter around the expected relation, and no significant positive correlation exists (Spearman correlation coefficient: $r = 0.47$; null-hypothesis probability: $p = 0.17$). Taking errors in x and y axes into account, we obtain a chi-squared of $\chi^2 = 73$ for 9 degrees of freedom.

Figure 7 shows the *reflionx* normalization as a function of the ionization parameter. It represents the parameters obtained in the fit of the ten observations. We can see that the *reflionx* normalization decreases significantly with the ionization parameter (Spearman correlation coefficient: $r = -0.71$; $p = 0.022$). We use the normalization instead of, for instance, the flux, because we are not interested in the physical meaning of parameter, but only in its evolution compared to its expected behavior.

Under the assumption of a fixed reflection factor, where the the ionization parameter and the power-law flux is known, the expected *reflionx* normalization can be deduced. Figure 7 represents the expected relation between the normalization and ξ. The normalization is not expected to vary a lot with the ionization parameter, because it should decrease with ξ if the power-law flux is fixed and increase with the power-law flux if ξ is fixed. We have seen that ξ increases with the power-law flux, so these two trends are added and compensate for each other, inducing a quasi-constant normalization.

Data obviously do not follow the expected behavior ($\chi^2 = 95$ for 10 degrees of freedom, which is significantly worse than the χ^2 found in the relation between ionization and power-law flux). This result shows a contradiction with the primary hypothesis of a constant reflection factor. In fact, data instead seem to follow the behavior expected for a fixed power-law flux ($\chi^2 = 12$ for 9 degrees of freedom), even though the power-law flux is strongly variable.

5.3. Varying R*

We see in Fig. 7 that the reflection factor cannot be constant. We therefore relax the assumption of a constant R^* and, for each observation, we determine the corresponding R^*. We use the method described in Sect. 5.1 again, using parameters values obtained by fitting data with the complete model. We plot the resulting R^* as a function of time in the top panel of Fig. 8. We can see that the reflection fraction is indeed varying over the observations and that it has a mean value of 4.99. The variability of the reflection factor is characterized by an rms fractional variability amplitude of 0.19 ± 0.03.

We plot R^* as a function of the power-law flux in the middle panel of Fig. 8 and as a function of the ionization parameter in the bottom panel. The reflection factor decreases when the power-law flux increases (Spearman correlation coefficient: $r = -0.73$; $p = 0.016$). This can be explained in the lamp-post model of Miniutti & Fabian (2004), which involves a source located on top of the accretion disk close to the black hole. In this model, changes in source height strongly affect the ratio between the flux emitted toward the observer and the flux emitted toward the accretion disk, because of light-bending effects in the strong gravitational field of the black hole. However, we do not see any correlation between the reflection factor and the ionization parameter in the bottom panel of Fig. 8 ($r = -0.37$; $p = 0.29$). A positive correlation is expected since the reflection factor is a measure of the flux hitting the accretion disk. Thus the pattern of the ionization changes does not match the prediction from the lamp-post configuration. We can also exclude any change in R^* stemming from changes in the inner radius, since $R_{\rm in}$ is found to remain constant at an extreme value of $1.235\ r_{\rm g}$.

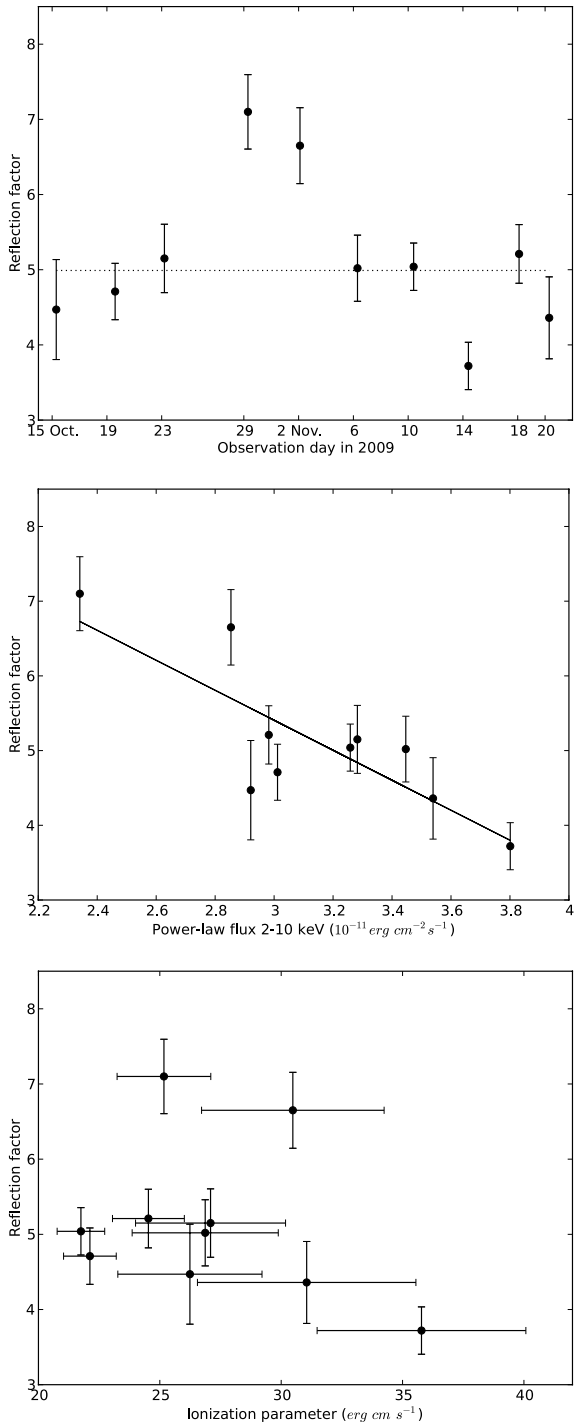

Fig. 8. Reflection factor determined for each of the ten observations of Mrk 509 using *reflionx* simulations with parameters values from the complete fitting. *Top panel*: R^* as a function of time. *Middle panel*: R^* as a function of the power-law flux. *Bottom panel*: R^* as a function of the ionization parameter.

6. Discussion

6.1. Ionized-reflection model parameters

We tested ionized-reflection models on the ten simultaneous *XMM-Newton* and INTEGRAL data of Mrk 509 using the *reflionx* XSPEC model. While *reflionx* does not provide a better fit to the soft-excess than does warm Comptonization (Mehdipour et al. 2011; Petrucci et al. 2013), a simple comparison of χ^2 is not sufficient to discard this model, because it may be simplified in a number of ways. We discuss here the physical consequences of applying this model to the Mrk 509 data set.

We first notice that the model predicts a very strong reflection (see top panel of Fig. 3) and low ionization, but underestimates the data at high energy. Such a strong reflection must dominate the hard X-ray spectrum over the power law, unlike what INTEGRAL shows, since it seems dominated by a power law. The failure to reproduce the high-energy emission, which is due to the large ionized reflection needed to reproduce the soft-excess is a severe difficulty for blurred ionized reflection models. Two factors may alleviate the difficulty. First,

the very low statistical weight of the INTEGRAL data compared to the *XMM-Newton* ones makes the fit rather insensitive to what happens at high energy, and it is possible that another solution producing a slightly worse overall fit could reproduce the INTEGRAL data better. In addition, we cannot exclude there being an additional component, like another, hard, power law that would start to dominate in the INTEGRAL domain, similar to the one observed by Maiolino et al. (2013) in Scorpius X-1, where they found evidence of a second component of Comptonization up to 200 keV.

Using a warm Comptonization model, it is possible to have a strong soft-excess without strong reflection, since these two spectral features come from two different components. Therefore, modeling the soft-excess with thermal Comptonization allows us to obtain a much better representation of the hard X-ray emission (see bottom panel of Fig. 3).

The ionized-reflection model used by Cerruti et al. (2011) gives a good fit for the Suzaku data between 15 and 30 keV. The fit with our ionized-reflection model (see Sect. 4.1) to the INTEGRAL data does not reproduce the high-energy spectrum as well. We first note that our data extend to much higher energy (20–140 keV). Furthermore, the flux between 17 and 60 keV measured during the INTEGRAL campaign ($6.368-6.371 \times 10^{-11}$ erg cm^{-2} s^{-1}) is significantly higher than the one during the Suzaku observations (4.81×10^{-11} erg cm^{-2} s^{-1}). Cerruti et al. (2011) also used a two-phase warm absorber, composed of models of partial covering absorption by partially ionized material, instead of the complex three-phase warm absorber derived from RGS data by Detmers et al. (2011). Doing so, the warm absorber is described with less precision in Cerruti et al. (2011) than in our model, leading to a different soft-excess, which results in stronger ionized reflection at high energy.

Since the ionization parameter required by the reflection component to fit the soft-excess is low, it cannot produce the (possibly relativistic) Fe XXV and Fe XXVI lines observed in Ponti et al. (2013). Instead it will contribute to the low ionization emission of the Fe Kα line at 6.4 keV. The Fe Kα line is observed to be composed of a narrow constant component and a resolved and variable component (Ponti et al. 2013), but there is no evidence of any relativistically smeared broad iron line in the EPIC spectra. This is also evident in the extreme parameters of *kdblur*, which effectively reduces the iron line to the absolute minimum, leaving only a very modest bump in the model. Such extreme values of *kdblur* parameters are needed to blur the photoionized emission from the accretion disk in order to reproduce the soft-excess.

We also tried to replace *reflionx* model by a new table model called *xillver* (García et al. 2013) to solve the underprediction of INTEGRAL data. This new version incorporates a richer atomic data base and is expected to provide a more accurate description of the iron Fe K emission line. Unfortunately, using this model did not improve the fit, so we kept the *reflionx* model for our analysis, as in Crummy et al. (2006).

During the fit, abundances of the *pexmon* model were fixed to solar value, as explained in Sect. 4.2. We have seen in Fig. 4 that if we leave abundances free to vary, we obtain a subsolar iron abundance of 0.28. This value is very problematic because, in the core of a galaxy, we would not expect to have underabundances compared to solar, owing to the abundance gradients in galaxies (Diaz 1989; Vila & Edmunds 1992; Zaritsky et al. 1994). For instance, Arav et al. (2007) found absolute abundances of two to three times solar in Mrk 279. We also note that Steenbrugge et al. (2011) have found relative abundances consistent with protosolar abundance ratios in Mrk 509.

The parameters obtained by fitting the data with the ionized-reflection model, such as the illumination index and the inner radius, have extreme values, implying an extreme geometry that maximizes relativistic effects. These parameters do in fact reach the model limits. We also obtain very low ionization values that do not seem standard. Indeed, among the objects analyzed by Crummy et al. (2006), 12 sources have been fitted with *kdblur* parameters similar to ours, i.e. an illumination index between 8.5 and 10 and an inner radius between 1.2 and 1.4. Only one object has a similar $\xi < 50$ erg cm s^{-1} ($\xi = 30$ erg cm s^{-1} in PG 1202+281), while all other objects have $\xi > 510$ erg cm s^{-1}, typical values being around 1600 erg cm s^{-1}.

6.2. Hypothesis of a stable geometry

We first tested the hypothesis of a stable geometry for Mrk 509, implying a constant reflection fraction R^* since implied distances are very small, and the reflector should react immediately to changes in the continuum. With this assumption, some relations are expected between the model parameters. The hypothesis does not hold because several of the expected relations are not recovered (see Sect. 5.2).

The ionization parameter shows scatter around the expected relation with the power-law flux (see Fig. 6). The assumption of constant R^* implies that the *reflionx* normalization is almost constant and independent of the ionization parameter (see Fig. 7). This is because, for a fixed ξ, the normalization will follow the power-law flux in order to maintain R^* constant, while for a fixed power-law flux, the normalization must decrease if the ionization increases. Both behaviors compensate for each other, which results in a flat relationship. Results of fitting of the ten observations with the complete model do not follow this expected trend, showing a clear anticorrelation between the normalization and the ionization, instead of the expected flat relationship. The normalization behaves as if the power-law flux is fixed, while it is strongly variable (see Fig. 5). We conclude that the *reflionx* model, if we assume a stable geometry, adjusts its parameters to compensate for changes of one parameter by variations in another one, fine-tuning them to fit the data. Doing so introduces an anticorrelation between the ionization parameter and the normalization, which is not physically justified.

6.3. Long time-scale variability of the soft-excess

We have seen in Fig. 2 that, on long time scales, the variability is maximum where the soft-excess dominates, while on short time scales, variability is minimum where reflection dominates. One possible parameter that could differentially affect soft and hard X-ray variability is the ionization. Indeed, effects of changes in ξ on the ionized reflection are most important in the energy range where ionized transitions are abundant, i.e. in the soft-excess. When the ionization state changes, the soft-excess flux varies strongly, which could explain the large variability on long time scales (Fig. 2), assuming that ξ is slowly varying.

The ionization parameter is defined as $\xi = \frac{L}{nr^2}$ erg cm s^{-1}. In the case of a stable geometry, r is also constant, and variations in the ionization parameter can only be due to changes in the density n of the disk, since ξ and L are not well correlated. We assume that an increase of the UV flux results from an increase in the accretion rate, hence an increase in the density. According to the ionization parameter definition, an increase in the density produces a decrease in the ionization. Thus the ionization parameter is expected to be anticorrelated with the UV flux.

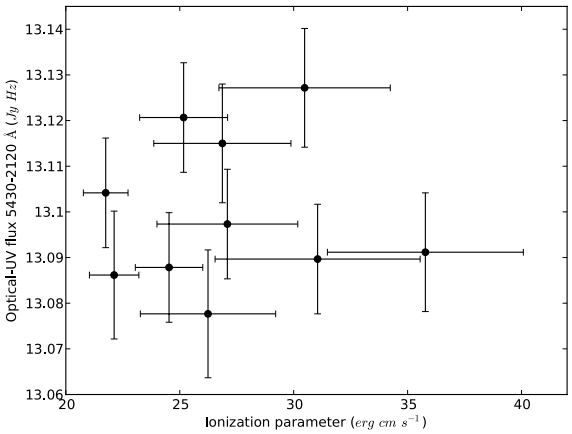

Fig. 9. Optical-UV flux (Mehdipour et al. 2011) as function of the ionization parameter estimated in this paper.

But this behavior is not observed in Fig. 9, which shows the optical-UV flux (Mehdipour et al. 2011) as a function of the ionization parameter (Spearman correlation coefficient: $r = 0.18$; $p = 0.63$). It therefore seems unlikely that the long term variations in the soft-excess are due to changes in ionization state resulting from changes in the density of the reflector.

6.4. Lamp-post configuration and light-bending effect

Since the stable geometry with constant reflection factor $R*$ is excluded, we drop this hypothesis and allow for a varying geometry. One such geometry is the lamp-post configuration, with light-bending effects taken into account (Miniutti & Fabian 2004). In this configuration, a primary source of X-rays is located close to a central black hole and illuminates both the observer at infinity and the accretion disk. When the height h of the source above the accretion disk varies, even if the intrinsic luminosity stays constant, the observed flux will vary. The reflection component is shown to vary with much smaller amplitude than the direct continuum (Miniutti & Fabian 2004). The low variability of the reflection implies that overall flux variability will be maximum where reflection features are weaker, i.e. between 2 keV and 5 keV. The variability on a short time scale does actually follow the expected behavior from the lamp-post configuration (see Fig. 2); however, another mechanism is needed to explain the long time-scale evolution of the soft-excess.

We calculated the reflection factor $R*$ for each observation (see top panel of Fig. 8). As expected, $R*$ is found to be variable, with a mean value of about 5. This high reflection factor again implies a reflection-dominated spectrum in hard X-rays, which is not supported by the INTEGRAL data. Theoretically, the lamp-post configuration allows $R*$ values much higher than 1, provided the source is very close to the black hole. From Fig. 5 in Miniutti & Fabian (2004), $R* \sim 5$ can be obtained if the height of the source above the disk is equal to $h \sim 1r_g$ (when the source is located on the rotation axis) or to $h \sim 2r_g$ (in the case of a corotating source at $2r_g$ from the axis). These are extreme geometries, implying maximally rotating (or close to maximally rotating) black holes. This conclusion does, however, agree with the extreme parameters of the *kdblur* model.

The middle panel of Fig. 8 shows that the reflection factor decreases when the power-law flux increases. The bottom panel of Fig. 5 also shows an anticorrelation between the ratio of the reflected flux over the power-law flux and the continuum flux, which provides similar information. This behavior is expected in the framework of the lamp-post configuration because, when the source comes closer to the disk, light-bending effect is stronger and induces more photons to be reflected on the accretion disk and less to illuminate the observer at infinity. In this case, we expect to find a correlation between the ionization parameter and the reflection factor because, when the height of the source h decreases, more light reaches the disk, increasing its ionization state. However, we find no correlation between $R*$ and ξ (see bottom panel of Fig. 8). As a consequence, similar to the case where the reflection factor is assumed to be constant, while the model is able to tune its parameters to fit the individual observations, the expected physical relations between the parameters are not present. This makes us conclude that ionized reflection – at least in these two configurations – is unlikely to be the correct explanation for the origin of the soft-excess in Mrk 509.

7. Conclusion

The nature of the soft-excess in AGN is still uncertain. While it can be fitted by both ionized reflection (Crummy et al. 2006; Zoghbi et al. 2008; Fabian et al. 2009; Ponti et al. 2010) and warm Comptonization (Magdziarz et al. 1998; Middleton et al. 2009; Jin et al. 2009; Mehdipour et al. 2011; Petrucci et al. 2013) in most, if not all, objects, some detailed features observed in individual objects point either to the former – lags in the soft-excess (Cackett et al. 2013; De Marco et al. 2011, 2013) in iron K and L lines (Fabian et al. 2009; Zoghbi et al. 2013; Kara et al. 2013) – or to the latter: correlation with UV or variability spectrum (Walter & Fink 1993; Edelson et al. 1996; Marshall et al. 1997; Mehdipour et al. 2011; Done et al. 2012). Because blurring can make ionized reflection look very featureless, the distinction between the two models at low energies is difficult and leads to a confusing situation about the origin of the soft-excess.

In this work we applied the blurred ionized-reflection model in Mrk 509, a bright Seyfert 1 galaxy for which we have a unique data set and which shows the presence of a strong soft-excess. The ionized-reflection model has some difficulty in fitting the broad-band spectrum of Mrk 509, even when assuming a very strong reflection and an extreme geometry. We first made the hypothesis of a stable geometry, but this configuration leads to a non-physical anticorrelation between the ionization parameter and the *reflionx* normalization and cannot explain the strong variability of the soft-excess on long time scales. The soft-excess variability cannot be explained by a varying geometry such as a lamp-post configuration either. Furthermore, even if light-bending effects can induce a high reflection factor value, we cannot find the expected correlation between $R*$ and ξ. The *reflionx* model fine-tunes its parameters in order to fit the data, introducing non-physical relations between parameters and preventing expected relations to appear. Ionized reflection is then unable to explain the origin of the soft-excess in Mrk 509.

In Mehdipour et al. (2011) and in Petrucci et al. (2013), the soft-excess of Mrk 509 was attributed to warm Comptonization based on some observed relationships, in particular the correlation between the UV and the soft X-ray fluxes. Under this hypothesis, the excess variability in the soft X-ray flux on long time scales can be explained by changes in the accretion rate (hence in the seed photon flux). This model of warm Comptonization therefore remains the most probable explanation of the soft-excess in this object.

Ionized reflection is expected as soon as a strong X-ray source irradiates very nearby cold-to-warm matter. Therefore, it is very possible that both mechanisms are at work in all objects, but the dominance of one over the other depends on the physical conditions of the disk and of the corona. The advent of sensitive telescopes in the hard X-rays such as NuSTAR and ASTRO-H in the future will provide very useful constraints on the origin of the soft-excess.

One physical parameter that can be expected to determine the existence of blurred ionized reflection is the Eddington ratio. Low Eddington ratios may indeed imply a transition from a standard accretion disk to an advection-dominated accretion flow (Ichimaru 1977; Rees et al. 1982; Narayan & Yi 1994, 1995a,b; Abramowicz et al. 1995), effectively truncating the accretion disk and removing cold material from the inner parts where relativistic effects are most important. This is supported further by the fact that the best evidence for blurred ionized reflection, including reverberation lags in the soft-excess (Cackett et al. 2013; De Marco et al. 2011) or iron L and K emission (Fabian et al. 2009; Zoghbi et al. 2013; Kara et al. 2013), are found in Narrow-Line Seyfert 1 objects (for instance, 1H 0707–495 and PG 1211+143), which are thought to have very high accretion rates. The moderate Eddington ratio of 0.3 in Mrk 509 may therefore be too low for blurred ionized reflection to become the dominant source of soft-excess in this object. However, lags have also been detected in many Seyfert galaxies without high accretion rates (De Marco et al. 2013).

The ten simultaneous *XMM-Newton* and INTEGRAL observations of Mrk 509 represent a unique data set that puts unprecedented constraints on the models. Many models are able to reproduce the soft-excess, because it is essentially featureless. Monitoring campaigns allow studying emission models along the time dimension and can provide very useful constraints to determine the origin of components like the soft-excess. Additional monitoring campaigns on other Seyfert 1 objects and, in particular, on narrow-line Seyfert 1 objects, where the evidence of ionized reflection is the strongest, would be very useful for understanding whether this component can really have different origins in different objects.

Acknowledgements. This work is based on observations obtained with *XMM-Newton*, an ESA science mission with instruments and contributions directly funded by ESA Member States and the USA (NASA). It is also based on observations with INTEGRAL, an ESA project with instrument and science data center funded by ESA member states (especially the PI countries: Denmark, France, Germany, Italy, Switzerland, Spain), Czech Republic, and Poland, and with the participation of Russia and the USA. R.B. acknowledges a grant from the Swiss Science National Foundation. G.P. acknowledges support via an EU Marie Curie Intra-European Fellowship under contract no. FP7-PEOPLE-2012-IEF-331095. P.O. Petrucci acknowledges financial support from the CNES and from the CNRS/PICS-INAF project. We thank the anonymous referee for comments and suggestions.

References

Abramowicz, M. A., Chen, X., Kato, S., Lasota, J.-P., & Regev, O. 1995, ApJ, 438, L37
Antonucci, R. 1993, ARA&A, 31, 473
Arav, N., Gabel, J. R., Korista, K. T., et al. 2007, ApJ, 658, 829
Arnaud, K. A., Branduardi-Raymont, G., Culhane, J. L., et al. 1985, MNRAS, 217, 105
Ballantyne, D. R., Iwasawa, K., & Fabian, A. C. 2001a, MNRAS, 323, 506
Ballantyne, D. R., Ross, R. R., & Fabian, A. C. 2001b, MNRAS, 327, 10
Ballantyne, D. R., Vaughan, S., & Fabian, A. C. 2003, MNRAS, 342, 239
Bianchi, S., Guainazzi, M., Matt, G., Fonseca Bonilla, N., & Ponti, G. 2009, A&A, 495, 421
Blandford, R. D., Netzer, H., Woltjer, L., Courvoisier, T. J.-L., & Mayor, M. 1990, Active Galactic Nuclei (Berlin: Springer-Verlag)
Bregman, J. N. 1990, A&ARv, 2, 125
Cackett, E. M., Fabian, A. C., Zogbhi, A., et al. 2013, ApJ, 764, L9
Cappi, M., Tombesi, F., Bianchi, S., et al. 2009, A&A, 504, 401
Cerruti, M., Ponti, G., Boisson, C., et al. 2011, A&A, 535, A113
Cooke, B. A., Ricketts, M. J., Maccacaro, T., et al. 1978, MNRAS, 182, 489
Crummy, J., Fabian, A. C., Gallo, L., & Ross, R. R. 2006, MNRAS, 365, 1067
De Marco, B., Ponti, G., Uttley, P., et al. 2011, MNRAS, 417, L98
De Marco, B., Ponti, G., Cappi, M., et al. 2013, MNRAS, 431, 2441
De Rosa, A., Piro, L., Matt, G., & Perola, G. C. 2004, A&A, 413, 895
Detmers, R. G., Kaastra, J. S., Steenbrugge, K. C., et al. 2011, A&A, 534, A38
Dewangan, G. C., Griffiths, R. E., Dasgupta, S., & Rao, A. R. 2007, ApJ, 671, 1284
Di Gesu, L., Costantini, E., Piconcelli, E., et al. 2014, A&A, 563, A95
Diaz, A. I. 1989, in Evolutionary Phenomena in Galaxies, eds. J. E. Beckman, & B. E. J. Pagel (Cambridge, New York: Cambridge University Press), 377
Done, C., Davis, S. W., Jin, C., Blaes, O., & Ward, M. 2012, MNRAS, 420, 1848
Edelson, R. A., Alexander, T., Crenshaw, D. M., et al. 1996, ApJ, 470, 364
Fabian, A. C., Ballantyne, D. R., Merloni, A., et al. 2002, MNRAS, 331, L35
Fabian, A. C., Miniutti, G., Iwasawa, K., & Ross, R. R. 2005, MNRAS, 361, 795
Fabian, A. C., Zoghbi, A., Ross, R. R., et al. 2009, Nature, 459, 540
García, J., Dauser, T., Reynolds, C. S., et al. 2013, ApJ, 768, 146
George, I. M., & Fabian, A. C. 1991, MNRAS, 249, 352
George, I. M., Turner, T. J., Netzer, H., et al. 1998, ApJS, 114, 73
Gierliński, M., & Done, C. 2004, MNRAS, 349, L7
Gondek, D., Zdziarski, A. A., Johnson, W. N., et al. 1996, MNRAS, 282, 646
Halpern, J. P. 1984, ApJ, 281, 90
Huchra, J., Latham, D. W., da Costa, L. N., Pellegrini, P. S., & Willmer, C. N. A. 1993, AJ, 105, 1637
Ichimaru, S. 1977, ApJ, 214, 840
Jaffe, W., Meisenheimer, K., Röttgering, H. J. A., et al. 2004, Nature, 429, 47
Jin, C., Done, C., Ward, M., Gierliński, M., & Mullaney, J. 2009, MNRAS, 398, L16
Kaastra, J. S., Petrucci, P.-O., Cappi, M., et al. 2011, A&A, 534, A36
Kara, E., Fabian, A. C., Cackett, E. M., et al. 2013, MNRAS, 434, 1129
Krolik, J. H. 1999, Active Galactic Nuclei: From the Central Black Hole to the Galactic Environment (Princeton Univ. Press)
Laor, A. 1991, ApJ, 376, 90
Magdziarz, P., & Zdziarski, A. A. 1995, MNRAS, 273, 837
Magdziarz, P., Blaes, O. M., Zdziarski, A. A., Johnson, W. N., & Smith, D. A. 1998, MNRAS, 301, 179
Maiolino, T., D'Amico, F., & Braga, J. 2013, A&A, 551, L2
Marshall, H. L., Carone, T. E., Peterson, B. M., et al. 1997, ApJ, 479, 222
Matt, G. 2001, in X-ray Astronomy: Stellar Endpoints, AGN, and the Diffuse X-ray Background AIP Conf. Proc., 599, 209
Matt, G., Perola, G. C., & Piro, L. 1991, A&A, 247, 25
Matt, G., Marinucci, A., Guainazzi, M., et al. 2014, MNRAS, 439, 3016
Mehdipour, M., Branduardi-Raymont, G., Kaastra, J. S., et al. 2011, A&A, 534, A39
Meisenheimer, K., Tristram, K. R. W., Jaffe, W., et al. 2007, A&A, 471, 453
Middleton, M., Done, C., Ward, M., Gierliński, M., & Schurch, N. 2009, MNRAS, 394, 250
Miller, L., Turner, T. J., Reeves, J. N., et al. 2007, A&A, 463, 131
Miller, L., Turner, T. J., & Reeves, J. N. 2008, A&A, 483, 437
Miniutti, G., & Fabian, A. C. 2004, MNRAS, 349, 1435
Morini, M., Lipani, N. A., & Molteni, D. 1987, ApJ, 317, 145
Morrison, R., & McCammon, D. 1983, ApJ, 270, 119
Nandra, K., George, I. M., Mushotzky, R. F., Turner, T. J., & Yaqoob, T. 1997, ApJ, 477, 602
Nandra, K., O'Neill, P. M., George, I. M., & Reeves, J. N. 2007, MNRAS, 382, 194
Narayan, R., & Yi, I. 1994, ApJ, 428, L13
Narayan, R., & Yi, I. 1995a, ApJ, 444, 231
Narayan, R., & Yi, I. 1995b, ApJ, 452, 710
Page, M. J., Davis, S. W., & Salvi, N. J. 2003, MNRAS, 343, 1241
Papadakis, I. E., Brinkmann, W., Gliozzi, M., et al. 2010, A&A, 510, A65
Perola, G. C., Matt, G., Cappi, M., et al. 2002, A&A, 389, 802
Peterson, B. M., Ferrarese, L., Gilbert, K. M., et al. 2004, ApJ, 613, 682
Petrucci, P.-O., Paltani, S., Malzac, J., et al. 2013, A&A, 549, A73
Piconcelli, E., Jimenez-Bailón, E., Guainazzi, M., et al. 2005, A&A, 432, 15
Ponti, G., Miniutti, G., Cappi, M., et al. 2006, MNRAS, 368, 903
Ponti, G., Cappi, M., Vignali, C., et al. 2009, MNRAS, 394, 1487
Ponti, G., Gallo, L. C., Fabian, A. C., et al. 2010, MNRAS, 406, 2591
Pinto, C., Kriss, G. A., Kaastra, J. S., et al. 2012, A&A, 541, A147
Ponti, G., Cappi, M., Costantini, E., et al. 2013, A&A, 549, A72
Pounds, K. A., Warwick, R. S., Culhane, J. L., & de Korte, P. A. J. 1986, MNRAS, 218, 685

Pounds, K. A., Nandra, K., Fink, H. H., & Makino, F. 1994, MNRAS, 267, 193
Pounds, K., Reeves, J., O'Brien, P., et al. 2001, ApJ, 559, 181
Poutanen, J., & Svensson, R. 1996, ApJ, 470, 249
Raban, D., Jaffe, W., Röttgering, H., Meisenheimer, K., & Tristram, K. R. W. 2009, MNRAS, 394, 1325
Rees, M. J., Begelman, M. C., Blandford, R. D., & Phinney, E. S. 1982, Nature, 295, 17
Ross, R. R., & Fabian, A. C. 1993, MNRAS, 261, 74
Ross, R. R., & Fabian, A. C. 2005, MNRAS, 358, 211
Sanders, D. B., Phinney, E. S., Neugebauer, G., Soifer, B. T., & Matthews, K. 1989, ApJ, 347, 29
Schurch, N. J., & Done, C. 2007, MNRAS, 381, 1413
Schurch, N. J., Done, C., & Proga, D. 2009, ApJ, 694, 1
Shakura, N. I., & Sunyaev, R. A. 1973, A&A, 24, 337
Singh, K. P., Garmire, G. P., & Nousek, J. 1985, ApJ, 297, 633
Steenbrugge, K. C., Kaastra, J. S., Detmers, R. G., et al. 2011, A&A, 534, A42
Tanaka, Y., Nandra, K., Fabian, A. C., et al. 1995, Nature, 375, 659
Tanaka, Y., Boller, T., Gallo, L., Keil, R., & Ueda, Y. 2004, PASJ, 56, L9
Turner, T. J., & Miller, L. 2009, A&ARv, 17, 47
Turner, T. J., & Pounds, K. A. 1989, MNRAS, 240, 833
Vaughan, S., & Fabian, A. C. 2004, MNRAS, 348, 1415
Vaughan, S., Edelson, R., Warwick, R. S., & Uttley, P. 2003, MNRAS, 345, 1271
Vila, M. B., & Edmunds, M. G. 1992, in The Stellar Populations of Galaxies, eds. B. Barbuy, & A. Renzini, IAU Symp., 149, 500
Walter, R., & Fink, H. H. 1993, A&A, 274, 105
Woo, J.-H., & Urry, C. M. 2002, ApJ, 579, 530
Zaritsky, D., Kennicutt, Jr., R. C., & Huchra, J. P. 1994, ApJ, 420, 87
Zdziarski, A. A., Johnson, W. N., Done, C., Smith, D., & McNaron-Brown, K. 1995, ApJ, 438, L63
Zdziarski, A. A., Johnson, W. N., & Magdziarz, P. 1996, MNRAS, 283, 193
Zhou, Y. Y., Yu, K. N., Young, E. C. M., Wang, J. M., & Ma, E. 1997, ApJ, 475, L9
Zoghbi, A., Fabian, A. C., & Gallo, L. C. 2008, MNRAS, 391, 2003
Zoghbi, A., Reynolds, C., Cackett, E. M., et al. 2013, ApJ, 767, 121